Energy Advances

ROYAL SOCIETY OF CHEMISTRY

PAPER

View Article Online
View Journal | View Issue

Cite this: *Energy Adv.*, 2026, 5, 448

Graphene oxide precursor effects on 3D-printed carbon scaffolds

Megan C. Freyman,†[a] Xinzhe Xue,†[b] Dun Lin,[b] Yat Li,[b] Marcus Worsley[a] and Swetha Chandrasekaran*[a]

Manganese oxide (MnO_2), an earth-abundant material, is a promising component for energy storage devices, with uses in both pseudocapacitors and batteries. However, high MnO_2 loading often leads to reduced performance due to poor ion diffusion. 3D printing, particularly using the direct ink writing (DIW) technique, offers a solution by enabling the fabrication of electrodes with hierarchical porous structures and open channels that enhance mass transport and ion diffusion. Previous work demonstrated that 3D-printed graphene aerogels with MnO_2 coatings exhibited excellent electrochemical performance, even with thick electrodes, due to their optimized structure. Building on this work, the current study investigates the performance differences between aerogels developed using graphene oxide (GO) and reduced graphene oxide (rGO) as carbon precursors. Both materials were incorporated into thixotropic inks, 3D-printed into lattice structures, and carbonized. Despite expected similarities between the final graphene aerogel, rGO-based aerogels exhibited superior areal capacitance, compared to GO-based aerogels. These differences are attributed to the lower oxygen content and defect density of rGO, which influence its interaction with cellulose viscosifiers in the ink formulation. Brunauer–Emmett–Teller (BET) surface area analysis revealed that rGO aerogels exhibit a larger surface area and mesoporous structure, further enhancing their performance. When coated with MnO_2, rGO-based aerogels maintained their superior capacitive behavior over GO-based aerogels. This study highlights the effect of carbon precursor on the end performance of graphene aerogels.

Received 28th April 2025,
Accepted 3rd March 2026

DOI: 10.1039/d5ya00116a

rsc.li/energy-advances

Introduction

As the demand for electrification increases, from small portable devices to large car batteries and grid-scale storage—energy storage device design must evolve. Pseudocapacitors are an attractive technology due to their fast charge and discharge rates and lightweight nature, although they have a lower energy storage density compared to batteries.[1,2] Manganese oxide (MnO_2) is a versatile material that can be used in both batteries and pseudocapacitors. MnO_2 is the most extensively studied transition metal oxide material for pseudocapacitors because of its high theoretical specific capacitance (1370 F g^{-1}).[3] The crystal structure of MnO_2 significantly influences its pseudocapacitive performance.[4] MnO_2 has been investigated as a potential cathode material due to its high theoretical energy density, attributed to a potential two-electron transfer mechanism.[5,6] However, MnO_2 has not been widely adopted as a cathode material for several reasons, including challenges associated with thicker layers that hinder charge transfer.[7] A previous study demonstrated that the performance of MnO_2 can be significantly enhanced by using a 3D printed graphene aerogel scaffold. The authors attributed this improvement to the hierarchical porous structure provided by the 3D printed carbon scaffold.[8] 3D printing offers a method to create components with custom architectures that can enhance the performance of the final product. In this paper, we employ the direct ink writing (DIW) 3D printing technique. DIW involves extruding a thixotropic ink layer by layer to construct a part. This technique allows for the deployment of custom inks during the printing process, enabling the creation of both unique architectures and functional materials.[8–11]

3D printed carbon aerogels offer a route to developing thicker electrodes for energy storage devices. By taking advantage of the inherent high surface area and porosity of the carbon aerogel, coupled with 3D printing, one can increase the thickness of an electrode without sacrificing performance due to mass transport limitations.[12] In a previous study by Yao *et al.*[8] carbon ink was used to generate 3D printed graphene aerogels (GAs), utilizing graphene oxide (GO) as the precursor, to demonstrate that a thick graphene aerogel electrode could

[a] *Material Science Department, Lawrence Livermore National Lab, Livermore, California, 94551, USA. E-mail: chandrasekar2@llnl.gov*
[b] *Department of Chemistry and Biochemistry, University of California, Santa Cruz California, 95064, USA*
† These authors contributed equally to this work.

help increase the loading of MnO_2 active material while still exhibiting good performance. The previous work[8] focused on optimizing the performance of MnO_2 electrodeposited onto a carbon aerogel scaffold. In contrast, the present study aims to improve the carbon scaffold itself, which supports the MnO_2. Our findings indicate that the choice of carbon precursor plays a role in the performance of the electrodeposited MnO_2.

We utilized reduced graphene oxide (rGO) as the precursor due to its lower oxygen content compared to a standard graphene oxide (GO) starting material. The rGO has 8% oxygen content compared to the GO which has 45–55% oxygen content.[13,14] The use of rGO, a graphene precursor with a lower starting oxygen content, presents a couple of benefits over GO. First, based on work by Qiu *et al.*, rGO allows the synthesis of a porous scaffold with finer pores and increased density.[15] This modified pore morphology should result in improved electrochemical performance and is the main focus of this work. Secondly, using rGO provides a path to produce printable inks that can be treated at lower temperature (<800 °C) to achieve acceptable conductivity. Lowering the processing temperature allows for the development of functionalized inks that are doped with a wider range of active materials for energy storage, catalysis, sensing, *etc.* Exploring this advantage is the focus of future work.

Here, we produced a conductive carbon scaffold through standard high temperature treatments (1000 °C) followed by electrodeposition of the active material. After the carbonization step, we expected the resulting graphene aerogel electrodes to be chemically similar. However, rGO-based electrodes exhibited superior electrochemical performance compared to GO-based electrodes. This difference in performance persists even when both types of carbon aerogel scaffolds are coated with MnO_2, with MnO_2-coated rGO electrodes achieving higher areal capacitance than their GO counterparts across all current densities we studied. We believe these electrochemical differences arise from the differences in pore morphology due to interactions between the graphene precursors (rGO and GO) and water during the freezing process.

Experimental

Synthesis of graphene oxide ink

An aqueous suspension of graphene oxide (40 mg mL^{-1}, Cheap Tubes) was prepared. To this suspension, 6 wt% hydroxypropyl methyl cellulose (Methocel Dow Chemicals) was added and mixed in a Flak Tech planetary mixer at 2500 rpm in one-minute increments until a smooth ink was generated.

Synthesis of reduced graphene oxide ink

An aqueous suspension of reduced graphene oxide (30 mg mL^{-1}, Cheap Tubes) was prepared with the addition of 5 wt% Pluronic F127 (Sigma Aldrich). To this suspension, 18 wt% cellulose nanocrystals (Celluforce) were added and mixed in a Flak Tech planetary mixer at 2500 rpm in one-minute increments until a smooth ink was generated.

Printing procedure

The inks were loaded into a 10 cc syringe (Nordson EFD) and centrifuged to remove bubbles. The ink was printed using an Aerotech A3200 Gantry Direct Ink Write System with a 400 μm nozzle (Nordson, Smooth Taper Nozzle) at a pressure of 18 psi. The printed samples were immediately frozen with dry ice, followed by liquid nitrogen, and then freeze-dried for 48 hours. After printing, the samples were carbonized under nitrogen with a ramp rate of 2 °C min^{-1} and held at 1000 °C for 3 hours.

MnO_2 coating

MnO_2 coatings on both 3D printed GO and rGO aerogels were prepared *via* an electrodeposition method. Specifically, the aqueous electrodeposition electrolyte is prepared by dissolving 0.1 M manganese acetate tetrahydrate (Thermo Scientific) into 30 mL Milli-Q water. The electrodeposition was performed using a two-electrode system where the working electrode was the GO or rGO printed aerogels, and the counter and reference electrodes were carbon paper. A constant current density of 10 mA cm^{-2} was applied for different time durations (5 mins and 2 hours). As a result, different mass loadings were achieved (2 mg cm^{-2} and 45 mg cm^{-2}). After deposition, the samples were washed with Milli-Q water and ethanol carefully and then dried at 70 °C in the air overnight.

The mass loadings (ML, mg cm^{-2}) of MnO_2 were calculated according to the following eqn (1):

$$\mathrm{ML} = \frac{\Delta m}{A} \quad (1)$$

where Δm (mg) is the mass difference after the deposition, and A is the coated area (cm^2).

Electrochemical testing

Cyclic voltammetry (CV), galvanostatic charge and discharge (GCD) and electrochemical impedance spectroscopy (EIS) were performed using a beaker cell with 3 M LiCl aqueous electrolyte for both single electrode and symmetric device measurements. Single electrode measurements were conducted in a three-electrode system, where the working electrode is GO or rGO aerogel, the counter electrode (CE) is a carbon rod, and the reference electrode (RE) is a saturated calomel electrode (SCE). For symmetric device measurements, electrodes were activated by scanning CV under 5 mV s^{-1} using a three-electrode-system. One electrode scan is stopped at 1 V *vs.* SCE, and the other electrode scan is stopped at 0 V *vs.* SCE. Then, both electrodes were assembled in a beaker cell as a device.

Compression testing

Compression testing was conducted using an Instron 5966 equipped with a 1 kilonewton load cell and compression platens. Monolith cubes measuring 1 cm × 1 cm × 1 cm were printed for each ink type and post-processed as described above. The dimensions and weight of the samples were recorded prior to compression studies. The samples were compressed at a rate of 1 mm s^{-1} to either 70% or 90% compression, depending on the specific experiment. Cyclic compression tests were also

performed, in which the sample was compressed in increments of 10% of its initial height until it reached 70% of the total height.

Surface area characterization

Nitrogen porosimetry was carried out using an Autosorb iQ. The sample was first degassed for 10 hours at 110 °C under vacuum. Surface area and pore distribution were determined by Brunauer–Emmett–Teller (BET) and Barrett–Joyner–Halenda (BJH) methods.[16,17]

Rheology testing

The rheology was collected using a TA instrument Discovery HR-1 hybrid rheometer. The ink was loaded onto 20 mm stainless steel parallel plates, with a Peltier plate geometry and a gap size of 500 μm. The experiments were run at room temperature.

Scanning electron microscopy

The SEM images of the bare printed aerogels were collected using a Thermo Fisher Scientific Apreo S LoVac scanning electron microscope, in standard mode using an EDT detector at a spot size of 8 and 10 kV. The SEM images of the MnO_2 deposited aerogels were collected using an FEI Quanta 3D dual-beam SEM.

X-Ray photoelectron spectroscopy

The surface chemical composition of the functional groups was investigated by X-ray photoelectron spectroscopy (XPS, Nexus X-ray Photoelectron Spectrometer) using monochromatic Al Kα X-ray (1486.6 eV) with a 400 μm spot size.

Results and discussion

GO and rGO printed aerogels are fabricated using a similar process. A suspension of the chosen carbon precursor is combined with a cellulose viscosifier to create a printable, water-based ink.

These inks are printed, immediately frozen, and then freeze-dried to preserve their porosity. Fig. 1 shows SEM images of the surface and cross-sections of the carbonized 3D-printed rGO and GO aerogel electrodes. rGO aerogels exhibit a more uniform pore structure, while GO aerogels feature a more irregular structure with small pores broken up by irregular large pores.

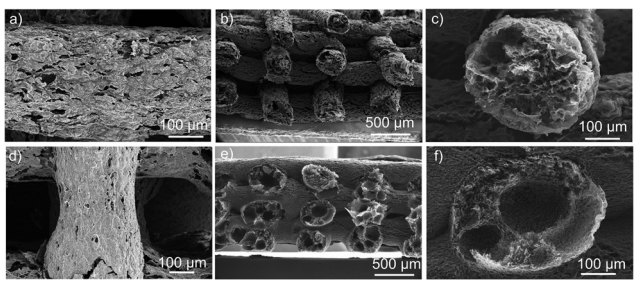

Fig. 1 SEM images of rGO and GO 3D printed aerogels. (a)–(c) The surface and cross-section of the printed rGO aerogel. (d)–(f) The surface and cross-section of the GO printed aerogel.

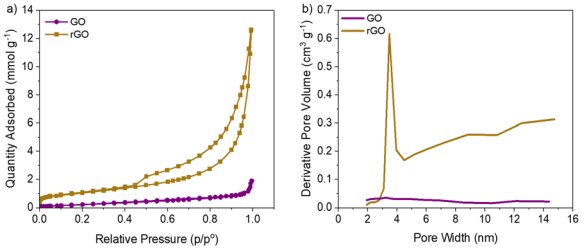

Fig. 2 (a) Nitrogen adsorption and desorption isotherms; and (b) pore size distribution for the rGO and GO printed aerogels.

Fig. 2 illustrates the pore distribution of bare rGO and bare GO aerogels made using the 3D printing ink formulation. The rGO aerogel achieves a surface area of 81.9 $m^2 g^{-1}$, while the GO aerogel has a significantly lower surface area of 17.7 $m^2 g^{-1}$. The hysteresis observed in the nitrogen sorption isotherm of the rGO sample (Fig. 2a) compared to that of the GO sample suggests an increase in mesopores in the rGO sample.[18,19] This is corroborated by the pore size distribution analysis (Fig. 2b), which shows a notable spike in porosity around 3.5 nm in the rGO sample compared to the GO sample.

Qiu *et al.* demonstrated that the C/O ratio in graphene freeze casting solutions can affect the ice crystal formation and resulting final pore structure of the aerogels. By decreasing the amount of oxygen, the interaction between the graphene sheets and the freezing front is weakened. Based on SEM images, Qiu *et al.* showed that this effect results in the pore size decreasing as the C/O ratio increases.[15,20] Based on the elemental characterization the C/O ratio for the GO precursor is 0.77 and the C/O ratio for rGO is 11.4.[13,14] Thus, the large increase in C/O going from GO to rGO should result in smaller pores in the rGO-based aerogel and in fact, the result in the present work is consistent with that in the published study by Qiu *et al.* SEM images show larger pores in the GO aerogel compared with the rGO aerogel (Fig. 1). This is also supported by BET measurements, as shown in Fig. 2. There is evidence of greater microporosity in the rGO aerogel's nitrogen adsorption spectrum compared to that of the GO aerogel.

For a material to be utilized in an energy storage device it needs to be able to withstand compressive stress. In a standard coin cell or pouch cell the internal components will experience pressure due to internal or external forces.[21] To provide insights into how the carbon scaffolds will survive in the energy storage devices we conducted compression studies.

Fig. 3 presents the cyclic compressive stress–strain curves for rGO and GO aerogels from 10% to 70% strain. These curves were obtained through the compression of 1 × 1 × 1 cm monolith cubes of the respective aerogels made using the same formulation as the 3D printed aerogels. The curves reveal distinctly different mechanical responses for the two materials. The rGO aerogel demonstrates more elastic behavior compared to the GO aerogel, which exhibits a longer plateau region in its stress–strain response. Additionally, the rGO curves maintain a

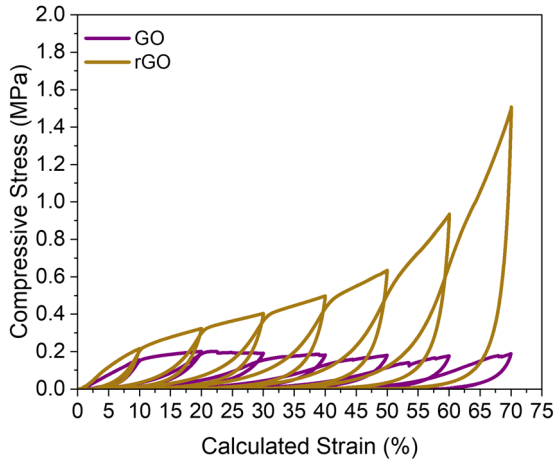

Fig. 3 Cyclic compressive stress–strain curves of rGO vs GO. The compressive curves start at 10% compression and the final compressive curve is 70%.

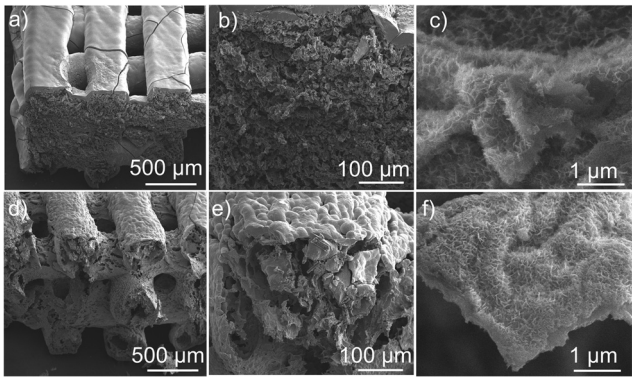

Fig. 4 SEM images of the 3D printed GO and rGO aerogels coated with 45 mg cm^{-2} MnO_2. (a)–(c) cross-section images of the MnO_2 coated rGO printed aerogel and (d)–(f) cross-section images of the MnO_2 coated GO printed aerogel.

relatively consistent shape during compressive cycling, in contrast to the behavior observed in the GO curves. Both the rGO and GO aerogels achieve similar specific moduli, 285 N m^{-3} and 212 N m^{-3} respectively. The differences in the stress–stain curves can be attributed to the difference in density of the sample, but the similarities in the specific moduli is due to the underlying chemical similarity of the carbon material.[22]

According to eqn (2), both rGO and GO aerogels are primarily influenced by bending and buckling behaviors.[23–25] We believe that the similarities in characteristics between the rGO and GO-based aerogels can be attributed to their underlying chemical similarities after carbonization. Eqn (2) is derived from the material composition of the aerogel being examined. For the rGO aerogels, the exponent was determined to be 2.75 ± 0.03, while for the GO aerogels, the exponent was found to be 2.62 ± 0.006.

$$\frac{\sigma_{pl}}{\sigma_{ys}} = \left(\frac{\rho}{\rho_s}\right)^2 \quad (2)$$

In eqn (2) σ_{pl} is the plateau stress (failure strength) of the carbon material (4500 MPa),[26] σ_{ys} is the experimental yield strength of the carbon aerogel (Fig. S7), ρ is the density of the material the foam is made of in this case carbon (2.26 g cm^{-3}),[27] and ρ_s is the experimental density of the carbon aerogel.

MnO_2 is an attractive pseudocapacitive material due to its high theoretical charge capacity.[6] However, as the thickness of MnO_2 increases, its performance decreases due to reduced mass transport. A previous study demonstrated that incorporating a 3D-printed carbon scaffold allows MnO_2 to maintain high electrochemical performance even at elevated mass loadings.[8] The 3D printed rGO and GO printed aerogels were coated with ε-MnO_2 through an electrodeposition method (Fig. 4), as reported previously.[8,28] By increasing the deposition time, the thickness of the MnO_2 layer increases. The thickness of the coating shown in Fig. 4 is approximately 45.2 mg cm^{-2}. The surface of the MnO_2 coating on the GO printed aerogels appears rougher compared to the coating on the rGO printed aerogels (Fig. 4a and d). As Fig. 4b and e show, the rGO filament has a more regular and dense pore structure, while the interior of the GO filament maintains a more irregular pore structure with large pores. Based on the SEM images in Fig. 4c and f, MnO_2 is deposited towards the center of the 3D printed filament in both the rGO and GO printed aerogels. The aerogels' high surface area is beneficial for constructing a high surface area MnO_2 layer to improve its pseudocapacitance. The structure of MnO_2 on the printed aerogels is similar for both rGO and GO.

We investigated how structural differences between rGO and GO aerogels affect their capacitive performance and their effectiveness as conductive scaffolds for pseudocapacitors. The rGO aerogel, with its higher surface area and rich mesoporous structures, increases both electric double layer capacitance (EDLC) and MnO_2 pseudocapacitance performance. Fig. 5 shows the electrochemical performance of single electrodes made from printed GO and rGO aerogels, both before and after MnO_2 coating. As shown in Fig. 5a, the rGO aerogel exhibits a longer discharge time than the GO aerogel, indicating substantially improved areal EDLC capacitance (Fig. 5b) benefitting from their rich and dense porous architectures. Both aerogels display a similar equivalent series resistance (ESR) of 5.0 Ohm and a steep slope in the low-frequency region of the electrochemical impedance spectrum (EIS), suggesting well-maintained good electrical conductivity and mass transfer resistance (R_{mt}).

We also evaluated rGO and GO electrodes with an MnO_2 loading of 2 mg cm^{-2}. Due to the higher surface area of rGO aerogels and effective MnO_2 infiltration within the rGO aerogel, the discharge time is significantly longer (Fig. 5d). As a result, the areal capacitance of the MnO_2-coated rGO aerogel reaches 1.1 F cm^{-2}, which is almost double that of the MnO_2-coated GO aerogel, which achieves 0.6 F cm^{-2} (Fig. 5e). EIS measurements confirm good ESR of 6.3 Ohm and low mass transfer resistance R_{mt}. We believe the enhanced performance is attributed to the dense porous structures and high surface area provided by the rGO aerogel scaffold.

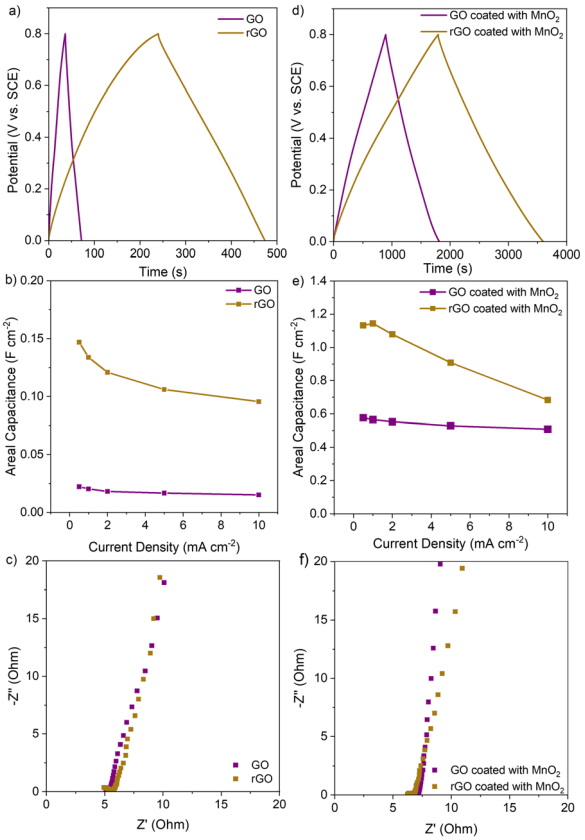

Fig. 5 Electrochemical performance of the 3D printed GO and rGO aerogel electrodes before and after coating MnO_2. (a) GCD curves at 0.5 mA cm^{-2}, (b) capacitance retention, and (c) EIS spectrum of the printed GO and rGO aerogels. (d) GCD curves at 0.5 mA cm^{-2}, (e) capacitance retention, and (f) EIS spectrum of printed GO and rGO aerogels coated with MnO_2.

Conclusions

In this study, two types of 3D printed aerogels were developed using different carbon precursors: graphene oxide (GO) and reduced graphene oxide (rGO). These materials were incorporated into a thixotropic ink for 3D printing. After carbonization, the rGO-based 3D printed aerogels demonstrated superior electrochemical performance. Compared to GO-based aerogels, the rGO-based aerogels exhibited $>3x$ higher areal capacitance up to 10 mA cm^{-2}. The enhanced performance of the rGO printed aerogels is attributed to their greater surface area and mesopore presence, as indicated by nitrogen porosimetry. Though both printed aerogel types showed bending-dominated behavior, the rGO based printed aerogels show more elastic behavior. When coated with MnO_2, the rGO printed aerogels electrochemically outperform the GO printed aerogels in terms of capacitive behavior. The study suggests that small differences in the carbon precursors significantly influence the physical and electrochemical properties of the printed aerogels. We believe that the increase in the C/O ratio from GO to rGO results in smaller pores in the rGO-based aerogel formed during freezing. This difference in porosity results in the ultimate difference in electrochemical performance. Future research will explore these differences using nuclear magnetic resonance (NMR) to better understand the chemical dynamics between the printed aerogel components.

Author contributions

Conceptualization: MW, SC, and YL. Funding acquisition: MW and SC. Investigation: SC, MF, XX, and DL. Writing – original draft: MF. Writing – reviewing and editing: SC, MF, MW, XX, and YL.

Conflicts of interest

There are no conflicts to declare.

Data availability

Supporting data and calculations can be found in the supplementary information (SI). Supplementary information is available. See DOI: https://doi.org/10.1039/d5ya00116a.

Acknowledgements

We thank T. Yuzvinsky from the University of California, Santa Cruz for SEM image acquisition. We also thank Kenedy Nguyen at the University of California, Merced for XPS data acquisition. This work was performed under the auspices of the U.S. Department of Energy by Lawrence Livermore National Laboratory under Contract DE-AC52-07NA27344, through LDRD award 23-SI-002.

Notes and references

1 R. Chen, M. Yu, R. P. Sahu, I. K. Puri and I. Zhitomirsky, *Adv. Energy Mater.*, 2020, **10**, 1903848.
2 P. Bhojane, *J. Energy Storage*, 2022, **45**, 103654.
3 Y. Hu, Y. Wu and J. Wang, *Adv. Mater.*, 2018, **30**, 1802569.
4 T. Yue, B. Shen and P. Gao, *Renewable Sustainable Energy Rev.*, 2022, **158**, 112131.
5 J. B. Goodenough and Y. Kim, *Chem. Mater.*, 2010, **22**, 587–603.
6 X. Guo, S. Yang, D. Wang, A. Chen, Y. Wang, P. Li, G. Liang and C. Zhi, *Curr. Opin. Electrochem.*, 2021, **30**, 100769.
7 Q.-Z. Zhang, D. Zhang, Z.-C. Miao, X.-L. Zhang and S.-L. Chou, *Small*, 2018, **14**, 1702883.
8 B. Yao, S. Chandrasekaran, J. Zhang, W. Xiao, F. Qian, C. Zhu, E. B. Duoss, C. M. Spadaccini, M. A. Worsley and Y. Li, *Joule*, 2019, **3**, 459–470.
9 X. Xu, Y. H. Tan, J. Ding and C. Guan, *Energy Environ. Mater.*, 2022, **5**, 427–438.
10 D. Lin, S. Chandrasekaran, J.-B. Forien, X. Xue, A. Pinongcos, E. Coester, M. A. Worsley and Y. Li, *Adv. Energy Mater.*, 2023, **13**, 2300408.

11 B. Yao, S. Chandrasekaran, H. Zhang, A. Ma, J. Kang, L. Zhang, X. Lu, F. Qian, C. Zhu, E. B. Duoss, C. M. Spadaccini, M. A. Worsley and Y. Li, *Adv. Mater.*, 2020, **32**, 1906652.
12 S. Chandrasekaran, D. Lin, Y. Li and M. A. Worsley, *Joule*, 2023, **7**, 866–883.
13 Reduced Graphene Oxide, https://www.cheaptubes.com/product/reduced-graphene-oxide/?srsltid=AfmBOopLGmNBys4LAmfwAZFzFOTlkNCGKutCVnSjPOmNY1OnzOfjjeKM, (accessed 29 January 2025).
14 Single Layer Graphene Oxide, https://www.cheaptubes.com/product/single-layer-graphene-oxide/?srsltid=AfmBOoo4NIrtS6jvQNnJRmAV4iQ_KP6HNCevGlm8c6t0_A5woF5Je1gC, (accessed 29 January 2025).
15 L. Qiu, J. Z. Liu, S. L. Y. Chang, Y. Wu and D. Li, *Nat. Commun.*, 2012, **3**, 1241.
16 S. Gregg and K. S. W. Sing, *Adsorption, surface area and porosity*, Academic Press, New York, 1982.
17 J. Rouquerol, F. Rouquerol, P. Llewellyn, G. Maurin and K. Sing, *Adsorption by powders and porous solids: principles, methodology and applications*, Academic Press, 2013.
18 K. Sing, *Colloids Surf., A*, 2001, **187–188**, 3–9.
19 M. A. Worsley, T. T. Pham, A. Yan, S. J. Shin, J. R. I. Lee, M. Bagge-Hansen, W. Mickelson and A. Zettl, *ACS Nano*, 2014, **8**, 11013–11022.
20 M. Li, Y. Zheng, H. Bai and W. Gao, *ACS Appl. Mater. Interfaces*, 2025, **17**, 19247–19262.
21 F. Dai and M. Cai, *Commun. Mater.*, 2022, **3**, 64.
22 M. Schwan and L. Ratke, *C*, 2016, **2**, 22.
23 Z. Qin, G. S. Jung, M. J. Kang and M. J. Buehler, *Sci. Adv.*, 2017, **3**, e1601536.
24 S. Chandrasekaran and R. Kumar, *Mater. Des.*, 2011, **32**, 4152–4163.
25 M. F. Ashby, *Philos. Trans. R. Soc., A*, 2005, **364**, 15–30.
26 M. Šilhavík, P. Kumar, Z. A. Zafar, M. Míšek, M. Čičala, M. Piliarik and J. Červenka, *Commun. Phys.*, 2022, **5**, 27.
27 J. Shim and K. A. Striebel, *J. Power Sources*, 2004, **130**, 247–253.
28 Y. Song, T. Liu, B. Yao, M. Li, T. Kou, Z.-H. Huang, D.-Y. Feng, F. Wang, Y. Tong, X.-X. Liu and Y. Li, *ACS Energy Lett.*, 2017, **2**, 1752–1759.